Available online at www.sciencedirect.com
ScienceDirect
European Journal of Mechanics B/Fluids 27 (2008) 110–130

Wave motions near a translating plate in a stratified fluid with infinite depth ☆

S.W. Joo [a,*], M.S. Park [b]

[a] *School of Mechanical Engineering, Yeungnam University, Gyongsan 712-749, South Korea*
[b] *Department of Engineering Science and Applied Mathematics, Northwestern University, Evanston, IL 60208, USA*

Received 4 August 2006; received in revised form 20 February 2007; accepted 27 March 2007

Available online 11 April 2007

Abstract

The dynamics of two horizontal inviscid liquid layers induced by a vertical wavemaker is studied analytically, followed by a numerical analysis. The focus is put on the time dependent motion of the two interfaces, formed between the two liquid layers and between the upper layer and the air above. The singularities that would appear in the two contact lines (the three-phase lines formed by the wavemaker, the liquids, and the air) in most variable-separating techniques are suppressed by a Fourier-integral method, which generates uniformly valid solutions; the surface elevations at the contact lines remain finite for all time. Various wavemaker velocities are considered for realistic applications of the results. The study is initially prompted by the oil-skimming problem, one of the main issues of which is to determine the optimum speed of the oil skirt, without leaving the spilt oil behind. By obtaining the locations of the two interfaces though this study, the motion of the oil layer (upper liquid) can be determined precisely, based on conservation laws.

Keywords: Wave motion; Invicid flow; Stratified fluid flow; Oil-skimming

1. Introduction

As a way of collecting spilt oil on the surface of sea water, partially-submerged structures, such as oil skirts, are often used. One of the more important things to consider for this oil collecting, or oil skimming, is making sure that the collected oil stays in the forward side of the translating structure. Without care, the oil can "climb" over the top of the structure or "leak" below the bottom edge, leaving the seawater behind contaminated. It is thus important to understand the dynamics of the oil layer with the translating structure and identify the conditions for the oil "climb" (oil flow over oil skirts) and "leak" (oil flow under oil skirts). If we assume that the oil-collecting structure is rigid, directed vertically, and translating horizontally, then the flow configuration is similar to that of a wavemaker problem with two superposed fluid layers.

☆ This work is supported by Yeungnam University.
* Corresponding author. Tel.: +82 53 810 2568; fax: +82 53 810 4627.
E-mail address: swjoo@yun.ac.kr (S.W. Joo).

0997-7546/$ – see front matter
doi:10.1016/j.euromechflu.2007.03.004

In most analyses of the wavemaker problem, viscous effects are ignored, and inviscid-irrotational flows are assumed. Peregrine [1] considered the wavemaker problem for an inviscid fluid with a finite depth. He linearized the problem by expanding the solutions for small time, and noted a logarithmic singularity at the contact line. Physically this singularity implied infinite vertical fluid velocity, or equivalently infinite surface elevation, at the contact line. He thus argued the necessity of a local solution near the contact line. There have been some disputes about the existence of the singularity by Chwang [2], for example, but it was confirmed by Lin [3] who approached the problem with a Lagrangian formulation of the governing system. The first successful local solution was reported by Roberts [4], who linearized the problem for small time and small Froude number. He noticed that near the contact line the depth of the fluid is not an appropriate length scale and that a self-similar solution exists. Joo et al. [5] reported a uniformly valid solution that matches with the self-similar solution near the contact line and outer solution away from the wavemaker. They also extended the solutions to include capillary effects at the free surface and the contact line. A careful matched asymptotic analysis is performed by King and Needham [6], who examined the initial development of a jet formed by a vertical wavemaker with constant acceleration. A uniformly valid small-time solution is thus obtained in the absence of capillary effects.

Wavemaker problems with two or more layers of fluids are investigated by many researchers, as summarized in the works by Rhodes-Robinson [7] and Sherief et al. [8]. For translating wavemakers fundamental difficulties associated with hydrodynamics near the contact lines remain the same. For applications to oil-skimming operations it is important to understand the dynamics of the oil layer, which is bounded by its free surface with the air and interface with seawater. Locations of the contact lines (wavemaker–air–oil and wavemaker–oil–seawater three-phase points) need to be accurately predicted for all time. One such study is performed by Joo and Park [9] for a wavemaker in finite-depth water. Precise dynamics of the free surface and the interface near the wavemaker are predicted for various wavemaker motions. The oil leak below the wavemaker, however, cannot be modeled because the wavemaker is fully submerged to the solid plate.

In this study we consider a finite vertical wavemaker translating horizontally in a layer of fluid with a finite depth placed on top of an infinite fluid, simulating the oil skimming with a finite draft in an infinite-depth seawater. In Section 2, mathematical formulation of the two-layer wavemaker problem is given. A method for obtaining uniformly valid solutions for two-layer wavemaker problem with any arbitrary wavemaker velocity is explained in Section 3. In Section 4 the method is used to obtain transient solutions for a number of wavemaker motions of interest. We conclude in Section 5 by summarizing the results.

2. Formulation

We consider the two-dimensional motion of two vertically stratified inviscid fluids of constant densities ρ_1 (lower) and ρ_2 (upper) induced by horizontal motion of a vertical wavemaker as shown in Fig. 1. Initially the wavemaker is at rest, so that the lower fluid infinite in depth and the upper fluid with a uniform thickness are both quiescent. The total submerged depth of the wavemaker is $d_1 + d_2$ initially. The wavemaker is then set in motion with a time-dependent velocity U, such as

$$U = Q\left[\left(\frac{d_1}{g}\right)^{1/2} t\right]^q, \tag{1}$$

where Q and q are constants and t is dimensionless time, scaled by $(d_1/g)^{1/2}$, here g is the gravitational acceleration. An impulsively started motion with a constant speed is described by setting $q = 0$ in the above equation, while a increasing wavemaker velocity with a constant acceleration Q is expressed by $q = 1$.

Since the motion of both fluids is started from rest, the flow stays irrotational according to Kelvin's theorem. Velocity potentials $\phi^{(1)}$ and $\phi^{(2)}$ then exist for the lower and the upper fluid layers, respectively, and must satisfy the Laplace equation for conservation of mass:

$$\phi^{(1)}_{xx} + \phi^{(1)}_{yy} = 0 \quad \text{for } x > s(t),\ y < \eta^{(1)}, \tag{2}$$

$$\phi^{(2)}_{xx} + \phi^{(2)}_{yy} = 0 \quad \text{for } x > s(t),\ \eta^{(1)} < y < \eta^{(2)}, \tag{3}$$

where the Cartesian coordinate system (x, y) is located at the initial wavemaker position with the y-coordinate starting from the interface between two fluid layers into the upper layer. All variables are nondimensionalized with $(gd_1)^{1/2}$

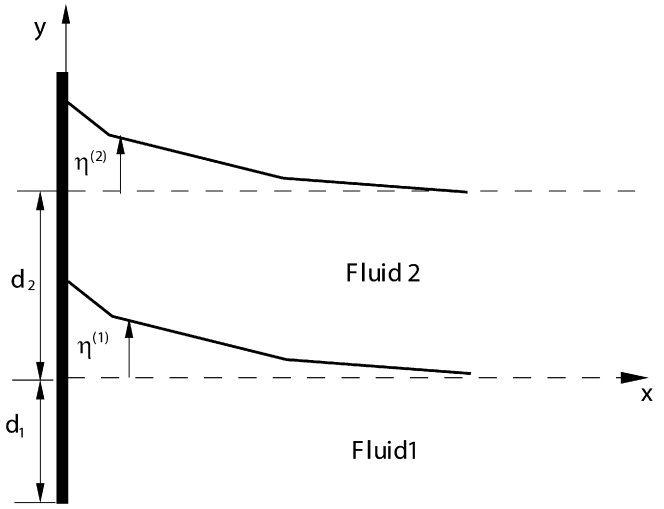

Fig. 1. Flow configuration for a two-layer wavemaker problem.

and d_1 as velocity and length scales, respectively. The travel distance of the wavemaker $s(t)$ is easily obtained by integrating the wavemaker velocity in time. The location of the interface $\eta^{(1)}$ between the upper and lower fluids and $\eta^{(2)}$ between the upper fluid and the passive air vary with time due to the motion of the wavemaker, and they can be obtained in coordination with the flow fields.

The horizontal components of the velocity vectors on the wavemaker are identical to that of the wavemaker:

$$\phi_x^{(1)} = \begin{cases} 0 & (y < -1), \\ & \text{on } x = s(t), \\ \alpha u(t) & (y > -1) \end{cases} \tag{4}$$

$$\phi_x^{(2)} = \alpha u(t) \quad \text{on } x = s(t), \tag{5}$$

where the Froude number α is defined as

$$\alpha = \frac{Q}{(g^{1+q} d_1^{1-q})^{1/2}}, \tag{6}$$

while that on the bottom is

$$\phi_y^{(1)} = 0 \quad \text{on } y = -\infty. \tag{7}$$

At the interface between the upper and the lower fluids, the jump in normal components of surface traction is balanced by the capillary force, which is written after dimensionless analysis as

$$\phi_t^{(1)} + \frac{1}{2}\left(\phi_x^{(1)2} + \phi_y^{(1)2}\right) + \eta^{(1)} - \rho\left[\phi_t^{(2)} + \frac{1}{2}\left(\phi_x^{(2)2} + \phi_y^{(2)2}\right) + \eta^{(1)}\right] = \frac{T_1 \eta_{xx}^{(1)}}{(1 + \eta_x^{(1)2})^{3/2}} \quad \text{on } y = \eta^{(1)}, \tag{8}$$

where the density ratio

$$\rho = \frac{\rho_2}{\rho_1} \ (\leqslant 1), \tag{9}$$

is taken to be no greater than unity, and the dimensionless surface tension is

$$T_1 = \frac{\sigma_1}{\rho_1 g d_1^2}, \tag{10}$$

where σ_1 is the surface tension coefficient at the interface, can be considered as the reciprocal of Bond number. The normal components of velocity vector must be continuous across the interface, so that

$$\phi_y^{(1)} - \phi_x^{(1)} \eta_x^{(1)} = \phi_y^{(2)} - \phi_x^{(2)} \eta_x^{(2)} \quad \text{on } y = \eta^{(1)}. \tag{11}$$

The interface location is defined by the kinematic condition as

$$\phi_y^{(1)} = \eta_t^{(1)} + \phi_x^{(1)}\eta_x^{(1)} \quad \text{on } y = \eta^{(1)}. \tag{12}$$

At the free surface between the upper fluid and the air, the dynamics of the air is ignored, and the dynamic surface condition on $y = h + \eta^{(2)}$ is written as

$$\phi_t^{(2)} + \frac{1}{2}\left(\phi_x^{(2)^2} + \phi_y^{(2)^2}\right) + \eta^{(2)} = \frac{T_2\eta_{xx}^{(2)}}{(1+\eta_x^{(2)^2})^{3/2}}, \tag{13}$$

where

$$h = \frac{d_2}{d_1} \tag{14}$$

is the ratio of thickness of the upper fluid to that of the lower fluid. Here, the dimensionless surface tension is

$$T_2 = \frac{\sigma_2}{\rho_2 g d_1^2}, \tag{15}$$

where σ_2 is the surface tension coefficient at the free surface. The kinematic condition here is

$$\phi_y^{(2)} = \phi_t^{(2)} + \phi_x^{(2)}\eta_x^{(2)} \quad \text{on } y = \eta^{(2)}. \tag{16}$$

As we have above, we will for convenience use the term "interface" for the interface between the upper and the lower fluids and "free surface" for the interface between the upper fluid and the air.

Initially, both fluids are at rest and the interfaces are planar, so that

$$\phi^{(1)} = \phi^{(2)} = 0 \quad \text{when } t < 0, \tag{17}$$

$$\eta^{(1)} = \eta^{(2)} = 0 \quad \text{when } t < 0. \tag{18}$$

Here it is assumed that static contact angles are 90 degrees at both contact lines [10,4].

In order to obtain uniformly valid solutions near the contact lines as well as away from the wavemaker, we perform a small Froude-number asymptotics by expanding velocity potentials and interface elevations for small α:

$$\phi^{(1)}(x,y,t) = \alpha\phi_1^{(1)}(x,y,t) + \alpha^2\phi_2^{(1)}(x,y,t) + \cdots, \tag{19}$$

$$\phi^{(2)}(x,y,t) = \alpha\phi_1^{(2)}(x,y,t) + \alpha^2\phi_2^{(2)}(x,y,t) + \cdots, \tag{20}$$

$$\eta^{(1)}(x,t) = \alpha\eta_1^{(1)}(x,t) + \alpha^2\eta_2^{(1)}(x,t) + \cdots, \tag{21}$$

$$\eta^{(2)}(x,t) = \alpha\eta_1^{(2)}(x,t) + \alpha^2\eta_2^{(2)}(x,t) + \cdots. \tag{22}$$

At both contact lines, dynamic contact angles are set to be equal to the static ones; interfaces meet wavemakers perpendicularly. A more general way of handling contact angles would be to prescribe the contact angles against contact-line velocity and to obtain contact-angle variations in couple with flow dynamics. The initial conditions equation (17) and the expansions equations (19)–(20) then must be modified.

If we substitute the above expansions for the velocity potentials and the interface elevations into the system of equations for both fluids in the previous section when expanding the boundary conditions at the interfaces about their mean locations, $y = 0$ and $y = h$, respectively, we can rearrange the entire equations in orders for $O(\alpha)$. The linearized equations in the leading order, $O(\alpha)$, are as follows. For convenience the subscript "1" indicating leading-order quantities will be omitted.

The leading-order velocity potentials still satisfy the Laplace equation:

$$\phi_{xx}^{(1)} + \phi_{yy}^{(1)} = 0 \quad \text{for } x > 0,\ y < 0, \tag{23}$$

$$\phi_{xx}^{(2)} + \phi_{yy}^{(2)} = 0 \quad \text{for } x > 0,\ 0 < y < h, \tag{24}$$

where the solution domains are now linearized. The boundary conditions on the wavemaker are

$$\phi_x^{(1)} = \begin{cases} 0 & (y < -1), \\ & \text{on } x = 0, \\ u(t) & (y > -1) \end{cases} \tag{25}$$

$$\phi_x^{(2)} = u(t) \quad \text{on } x = 0, \tag{26}$$

and that on the bottom surface is

$$\phi_y^{(1)} \to 0 \quad \text{on } y = -\infty. \tag{27}$$

At the interface between the upper and the lower fluids, the linearized boundary conditions are

$$\phi_t^{(1)} + \eta^{(1)} - \rho\left(\phi_t^{(2)} + \eta^{(1)}\right) - T_1\eta_{xx}^{(1)} = 0 \quad \text{on } y = 0, \tag{28}$$

$$\phi_y^{(1)} = \phi_y^{(2)} \quad \text{on } y = 0, \tag{29}$$

$$\eta_t^{(1)} = \phi_y^{(1)} \quad \text{on } y = 0. \tag{30}$$

At the free surface between the upper fluid and the air, they are

$$\phi_t^{(2)} + \eta^{(2)} - T_2\eta_{xx}^{(2)} \quad \text{on } y = h, \tag{31}$$

$$\eta_t^{(2)} = \phi_y^{(2)} \quad \text{on } y = h. \tag{32}$$

3. Transform solutions

We seek for the solution $\phi^{(1)}$ and $\phi^{(2)}$ as Fourier cosine transforms:

$$\phi^{(1)} = \frac{2}{\pi}\int_0^\infty \Phi^{(1)}\cos(kx)\,\mathrm{d}k, \qquad \phi^{(2)} = \frac{2}{\pi}\int_0^\infty \Phi^{(2)}\cos(kx)\,\mathrm{d}k \tag{33}$$

and

$$\eta^{(1)} = \frac{2}{\pi}\int_0^\infty B(k,t)\cos(kx)\,\mathrm{d}k, \qquad \eta^{(2)} = \frac{2}{\pi}\int_0^\infty D(k,t)\cos(kx)\,\mathrm{d}k, \tag{34}$$

and we obtain governing equations

$$\Phi_{yy}^{(1)} - k^2\Phi^{(1)} = \begin{cases} 0 & (y < -1), \\ u(t) & (y > -1), \end{cases} \tag{35}$$

$$\Phi_{yy}^{(2)} - k^2\Phi^{(2)} = u(t), \tag{36}$$

and boundary conditions

$$\Phi_y^{(2)} = D_t(k,t) \quad \text{at } y = h, \tag{37}$$

$$\Phi_t^{(2)} + \left(1 + T_2k^2\right)D(k,t) = 0 \quad \text{at } y = h, \tag{38}$$

$$\Phi_y^{(1)} = B_t(k,t) \quad \text{at } y = 0, \tag{39}$$

$$\Phi_t^{(1)} + B(k,t) - \rho\left(\Phi_t^{(2)} + B(k,t)\right) + T_1k^2B(k,t) = 0 \quad \text{at } y = 0, \tag{40}$$

$$\Phi_y^{(1)} = \Phi_y^{(2)} \quad \text{at } y = 0, \tag{41}$$

$$\Phi_y^{(1)} \to 0 \quad \text{at } y \to -\infty. \tag{42}$$

Considering Eqs. (41)–(42), we write general solutions to Eqs. (35)–(36) as

$$\Phi^{(1)} = \begin{cases} A(k,t)\mathrm{e}^{ky} - \frac{u(t)}{2k^2}\,\mathrm{e}^{k}\mathrm{e}^{ky} & \text{for } y < -1, \\ A(k,t)\mathrm{e}^{ky} - \frac{u(t)}{k^2}(1 - \frac{\mathrm{e}^{-k}}{2}\,\mathrm{e}^{-ky}) & \text{for } y > -1, \end{cases} \tag{43}$$

$$\Phi^{(2)} = C(k,t)\cosh(ky) - A(k,t)\mathrm{e}^{-ky} - \frac{u(t)}{k^2}\left(1 - \frac{\mathrm{e}^{-k}}{2}\,\mathrm{e}^{-ky}\right). \tag{44}$$

The free surface and interface boundary conditions equations (37)–(41) then yield a coupled system of equations for A, B, C and D:

$$k\mathrm{e}^{-kh}A + k\sinh(kh)C - \frac{u(t)}{2k}\mathrm{e}^{-k}\mathrm{e}^{-kh} = D_t, \tag{45}$$

$$-\mathrm{e}^{-kh}A_t + \cosh(kh)C_t + \frac{u'(t)}{2k^2}\mathrm{e}^{-k}\mathrm{e}^{-kh} - \frac{u'(t)}{k^2} + \gamma_2 D = 0, \tag{46}$$

$$kA - \frac{u(t)}{2k}\mathrm{e}^{-k} = B_t, \tag{47}$$

$$(1+\rho)A_t - \rho C_t\frac{(1-\rho)u'(t)}{k^2}\left(\frac{\mathrm{e}^{-k}}{2} - 1\right) + \gamma_1 B = 0, \tag{48}$$

where

$$\gamma_1 = 1 - \rho + T_1k^2, \qquad \gamma_2 = 1 + T_2k^2. \tag{49}$$

The Fourier coefficients B and D can be eliminated between Eqs. (45)–(46) and Eqs. (47)–(48), respectively, yielding equations for A and C. We then eliminate C to obtain a single fourth-order ordinary differential equation for A:

$$a_1A_{tttt}(k,t) + a_2A_{tt}(k,t) + a_3A(k,t) = R(k,t), \tag{50}$$

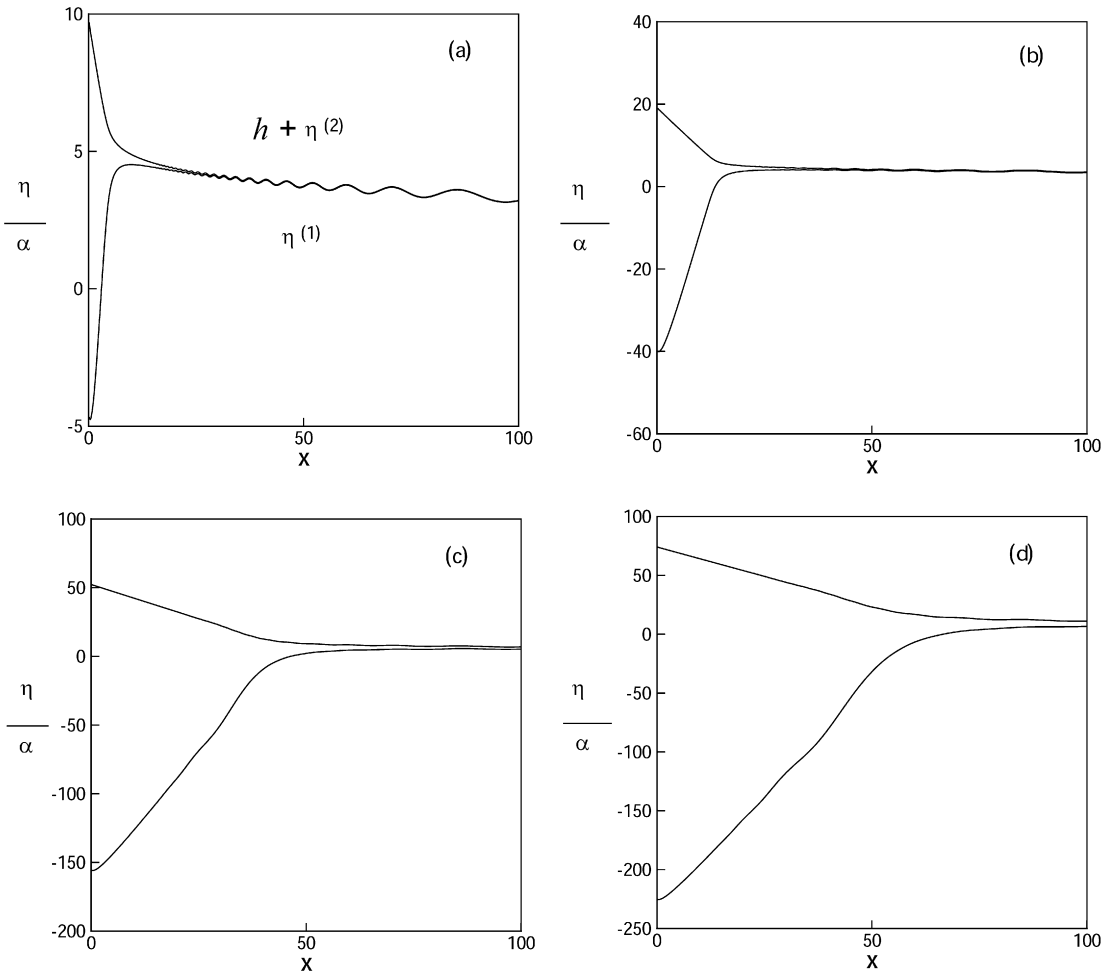

Fig. 2. Interface and free surface configuration for $u(t) = t$ when $t = 100$, $T_1 = 2\times10^6$, $T_2 = 2T_1$ and $\rho = 0.8$. (a) $h = 0.01$; (b) $h = 0.1$; (c) $h = 1$; (d) $h = 2$.

where

$$a_1 = 1 + \rho \tanh(kh), \tag{51}$$

$$a_2 = k\big[\gamma_1 + \gamma_2\big(\rho + \tanh(kh)\big)\big], \tag{52}$$

$$a_3 = k^2 \gamma_1 \gamma_2 \tanh(kh), \tag{53}$$

$$R(k,t) = \frac{u(t)}{2}\,\mathrm{e}^{-k}\gamma_1\gamma_2\tanh(kh) + \frac{u''(t)}{k}\left[\frac{\mathrm{e}^{k}}{2}\gamma_1 + \gamma_2(1-\rho)\tanh(kh) + \frac{\gamma_2\mathrm{e}^{-k}}{2}\big(\rho - \tanh(kh)\big)\right] + \frac{u'''(t)}{k^2}\left[1 - \rho + \frac{\mathrm{e}^{k}}{2}\big(\rho\tanh(kh) - 1\big) + \frac{\rho}{\cosh(kh)}\right]. \tag{54}$$

Eq. (50) has a general solution

$$A = A_p(k,t) + c_1(k)\sin(\beta_1 t) + c_2(k)\cos(\beta_1 t) + c_3(k)\sin(\beta_2 t) + c_4(k)\cos(\beta_2 t), \tag{55}$$

where

$$\beta_1 = \left(\frac{a_2 - \sqrt{a_2 - 4a_1a_3}}{2a_1}\right)^{1/2}, \qquad \beta_2 = \left(\frac{a_2 + \sqrt{a_2 - 4a_1a_3}}{2a_1}\right)^{1/2}. \tag{56}$$

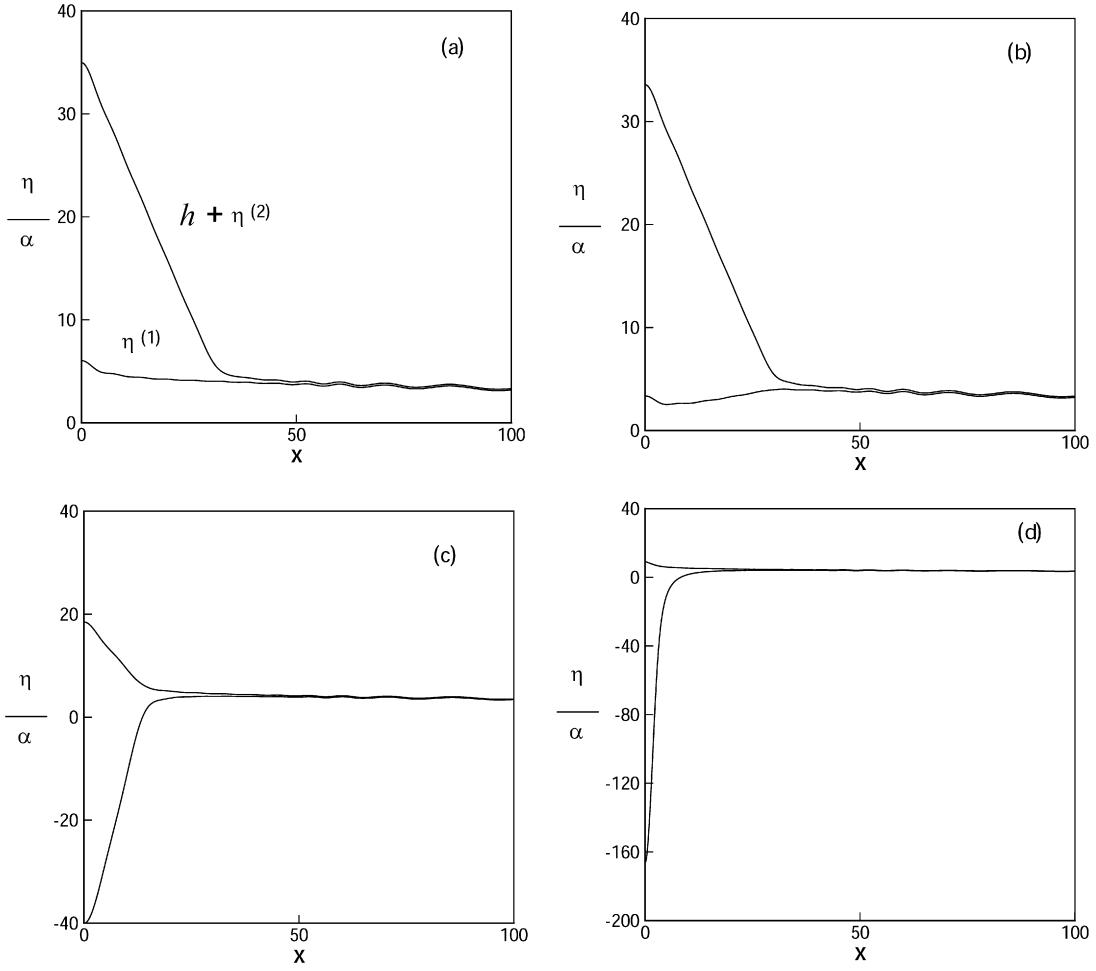

Fig. 3. Interface and free surface configuration for $u(t) = t$ when $t = 100$, $T_1 = 2 \times 10^6$, $T_2 = 2T_1$ and $h = 0.1$. (a) $\rho = 0.01$; (b) $\rho = 0.1$; (c) $\rho = 0.8$; (d) $\rho = 0.99$.

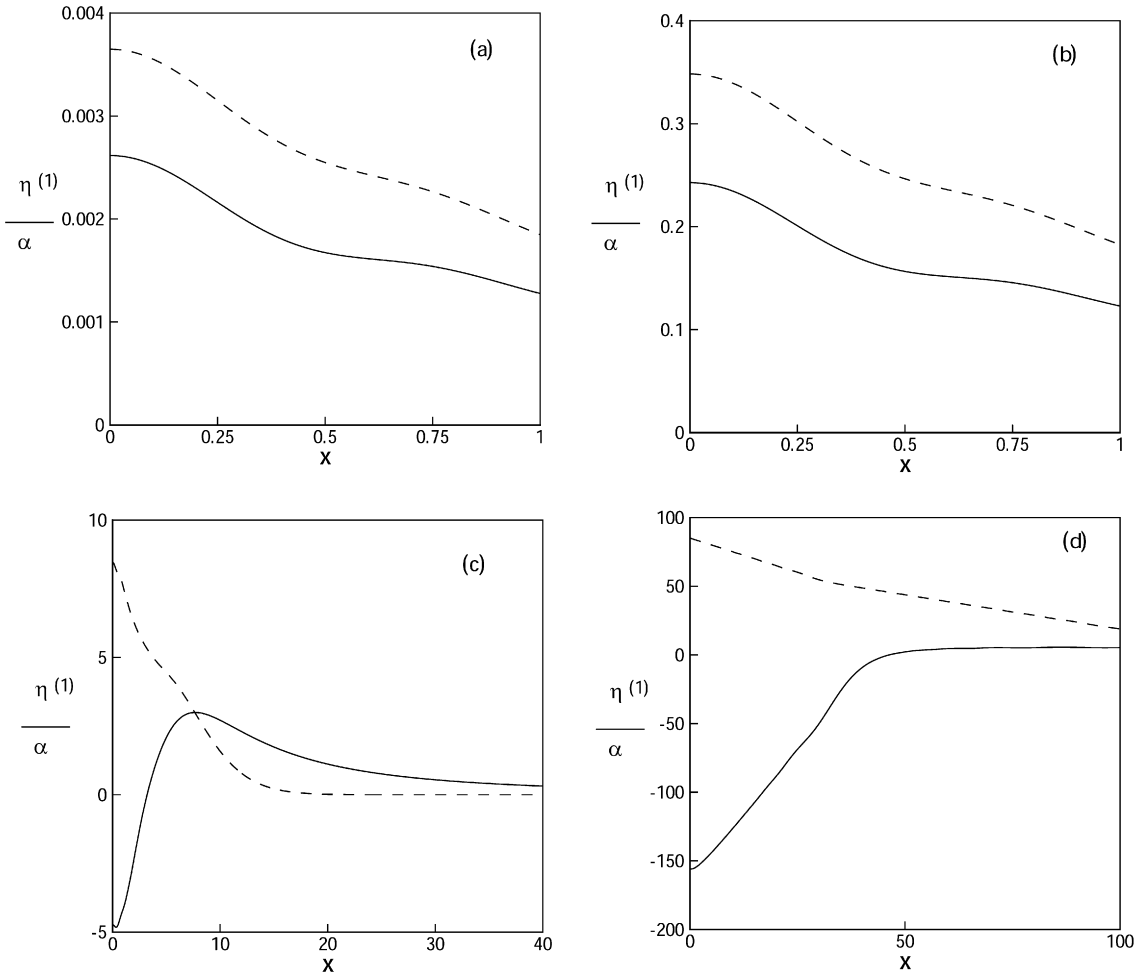

Fig. 4. Interface configuration for $u(t) = t$ when $\rho = 0.8$, $T_1 = 2 \times 10^6$, $T_2 = 2T_1$ and $h = 1$. (a) $t = 0.1$; (b) $t = 1$; (c) $t = 10$; (d) $t = 100$: finite depth (dash line) and infinite depth (solid line).

Here, A_p is a particular solution of Eq. (50) for a given q, and c_i $(i = 1, 2, 3, 4)$ are determined from the initial conditions.

The initial conditions for the interface elevations $\eta^{(1)}$ and $\eta^{(2)}$ can be converted into those for $\phi^{(1)}$ and $\phi^{(2)}$ through Eqs. (33) and (34). The appropriate initial conditions are then

$$\Phi^{(1)} = 0, \quad \Phi_t^{(1)} = \rho \Phi_t^{(2)} \quad \text{on } y = 0,\ t = 0 \tag{57}$$

and

$$\Phi^{(2)} = 0, \quad \Phi_t^{(2)} = 0 \quad \text{on } y = h,\ t = 0. \tag{58}$$

These conditions are easily converted in turn into those for $A(k, 0)$. The solution for $A(k, t)$ then is completely determined, after which that for $C(k, t)$ and consequently those for B and D are obtained; the time-dependent configurations for the interface and the free surface are determined in terms of Fourier integrals.

4. Calculations of surface and interface motions

Application of the aforementioned method for a particular oil skirt or wavemaker motion requires prescription of the velocity $u(t)$. In this section we choose three $u(t)$'s of practical interest, and examine the corresponding motions of the surface and the interface, including the dynamics of the contact lines. For readers interested in the mathematical expressions of the results some key solutions are listed in Appendix A.

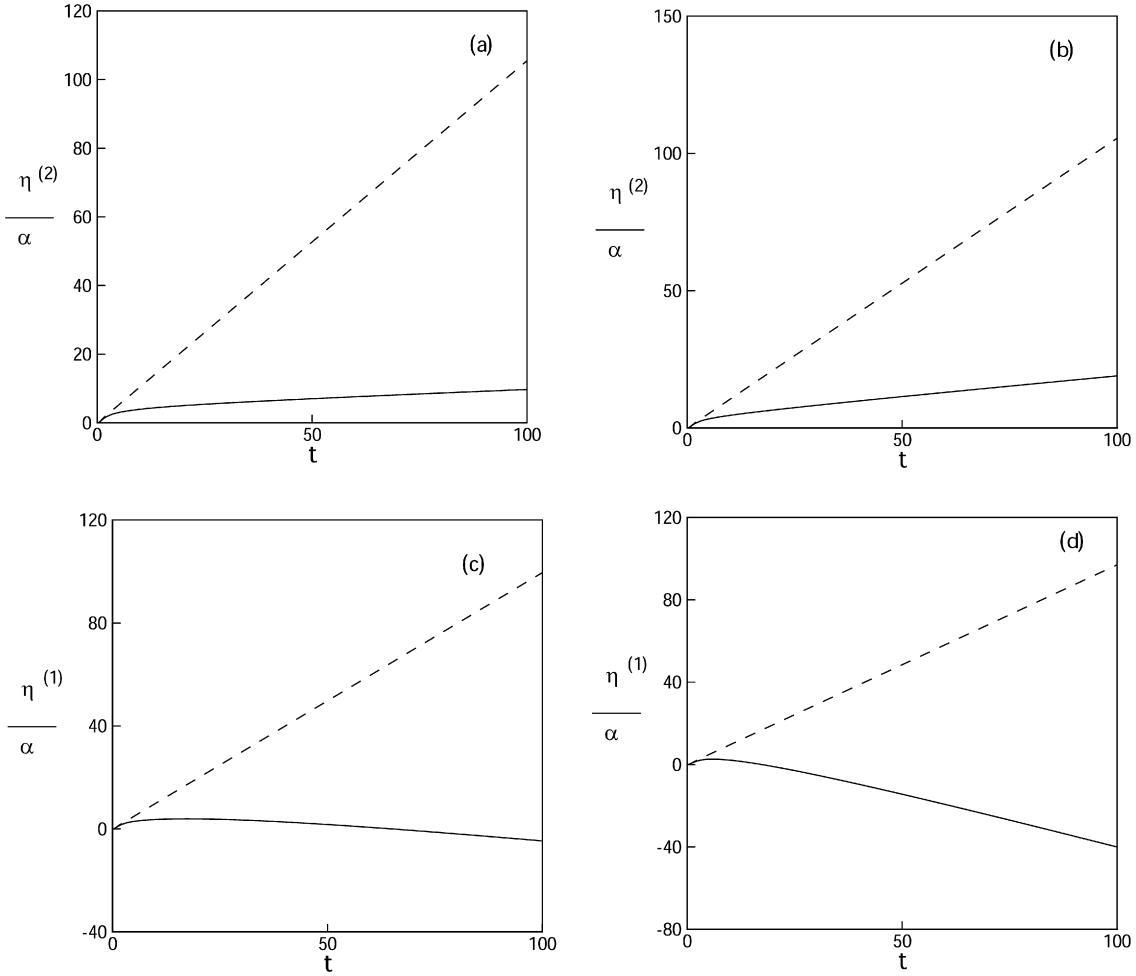

Fig. 5. Contact-line elevation for $u(t) = t$ with $\rho = 0.8$, $T_1 = 2 \times 10^6$, $T_2 = 2T_1$: (a) and (c) $h = 0.01$ with finite depth (- - -), infinite depth (—), (b) and (d) $h = 0.1$ with finite depth (- - -), infinite depth (—).

The integral of $\eta^{(1)}$ and $\eta^{(2)}$ is evaluated numerically as the sum of integrals from zero to M and M to infinity. The value for M is selected to be as large as 10^5 for small x and t, and as small as 10^{-1} when either x or t is large. The integral from zero to M is evaluated using 10-point Gauss-Quadrature and 21-points Kronrod formulae on both halves of the adaptive subintervals. The selection of the subinterval is based on the maximum absolute error estimate of 10^{-9}. Owing to the rapid oscillation of the integrand, the integral from M to infinity is obtained using Filon's Method [11].

In Figs. 2–7, $u(t) = t$; the wavemaker starts from rest and speeds up linearly in time. In Fig. 2 the density ratio is fixed at $\rho = 0.8$, a representative value for water and typical petroleum oil. The thickness ratio h is varied from 0.01 to 2. As the thickness of the upper fluid increases, the elevation of the interface becomes more pronounced, and the change of thickness of upper fluid is rarely significant, which means that the thickness of upper fluid layer is significantly deformed in a short distance for small h rather than for larger h, so that the lower fluid is more unlikely to leak under the wavemaker in case of smaller h while the upper fluid is easier to leak under the wavemaker in case of larger h. Therefore, in general sense of oil-skimming structure the longer wavemaker is demanded to prevent oil leaking or oil climbing from the oil skirts for larger h. For smaller h, as shown in Fig. 2(a), the interface configuration far from the wavemaker is quickly stable, which result agrees with Joo at al. [5] while for larger h, as shown in Fig. 2(d), the interface elevation far from the wavemaker is still high, so more oil climbing and oil leaking is expected with large t.

Fig. 3 shows the interface and free surface configuration at $t = 100$ when the thickness of upper fluid layer is of the small length of wavemaker immersed in lower-layer fluid ($h = 0.1$). The density ratio ρ is varied from 0.01

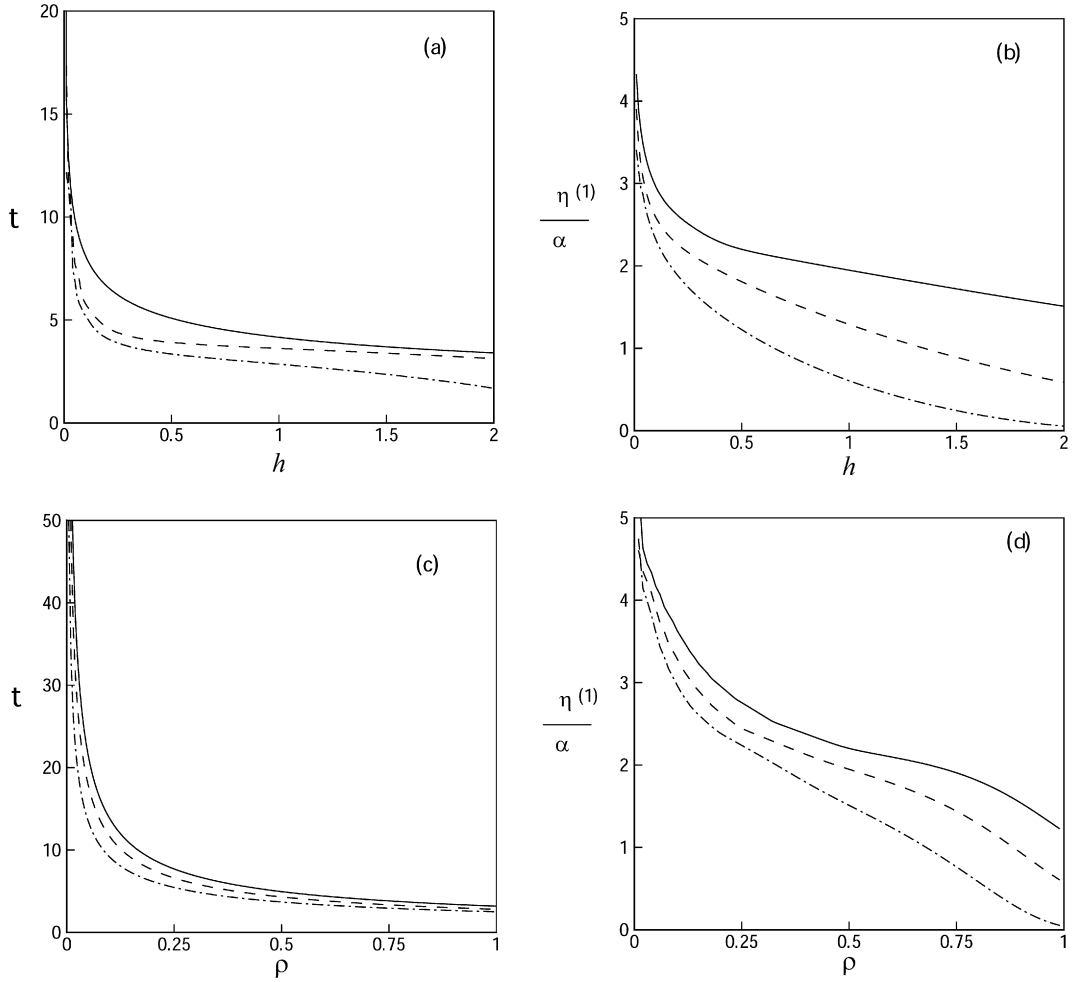

Fig. 6. Interface configuration for $u(t) = t$ with $T_1 = 2 \times 10^6$, $T_2 = 2T_1$: (a) Peak time (t) with respect to h when $\rho = 0.5$ (—), $\rho = 0.8$ (- - -), $\rho = 0.99$ (– · –); (b) Peak location ($\eta^{(1)}/\alpha$) with respect to h when $\rho = 0.5$ (—), $\rho = 0.8$ (- - -), $\rho = 0.99$ (– · –); (c) Peak time (t) with respect to ρ when $h = 0.5$ (—), $h = 1$ (- - -), $h = 2$ (– · –); (d) Peak location ($\eta^{(1)}/\alpha$) with respect to ρ when $h = 0.5$ (—), $h = 1$ (- - -), $h = 2$ (– · –).

(lighter upper fluid) to 0.99 (upper and lower fluid similar in density). Considering that the density is the only physical property distinguishing the two inviscid fluids and that only hydrodynamically stable stratifications are required for the initial conditions, we do not take density ratio equal or higher than unity. When ρ is very small as shown in Fig. 3(a), the upper fluid behaves like passive air against the lower fluid, so that the elevation of upper layer near $x = 0$ is higher and the upper fluid is likely to climb over the wavemaker, and the elevation of lower fluid moves as that of a single fluid layer, which agrees with Joo at al. [5]. On the other hand, when ρ is similar to unity as shown in Fig. 3(d), unlike Fig. 3(a), the elevation of low layer near $x = 0$ becomes lower, so that the upper fluid is likely to leak under the wavemaker, and the dynamics of the upper fluid is similar to the movement of a single fluid layer, which agrees with Joo at al. [5]. It is examined that the upper-layer fluid in Fig. 3(a) and the lower-layer fluid in Fig. 3(d) show similar behavior each, with appropriate re-scaling of length. However, the change of the thickness of upper layer in Fig. 3(d) becomes more stable in a short distance comparing with Fig. 3(a), and the amount of oil leaking in Fig. 3(d) is much larger than that of oil climbing in Fig. 3(a). Therefore, to prevent leaking or climbing in each density ratio, the position of the wavemaker submerged in the two layers has to be adjusted according to ρ, especially in case of high ρ.

Fig. 4 shows the interface and free surface configuration at different t for finite depth [9] (dash line) and infinite depth (solid line) with $\rho = 0.8$ and $h = 1$. The figures are useful to determine when the upper-layer fluid is going to leak under the wavemaker and to understand each characteristics between two cases. For t is small, for example $t = 0.1$ and $t = 1$, the wave patterns are similar each other, which means that the lower fluid does not leak under the

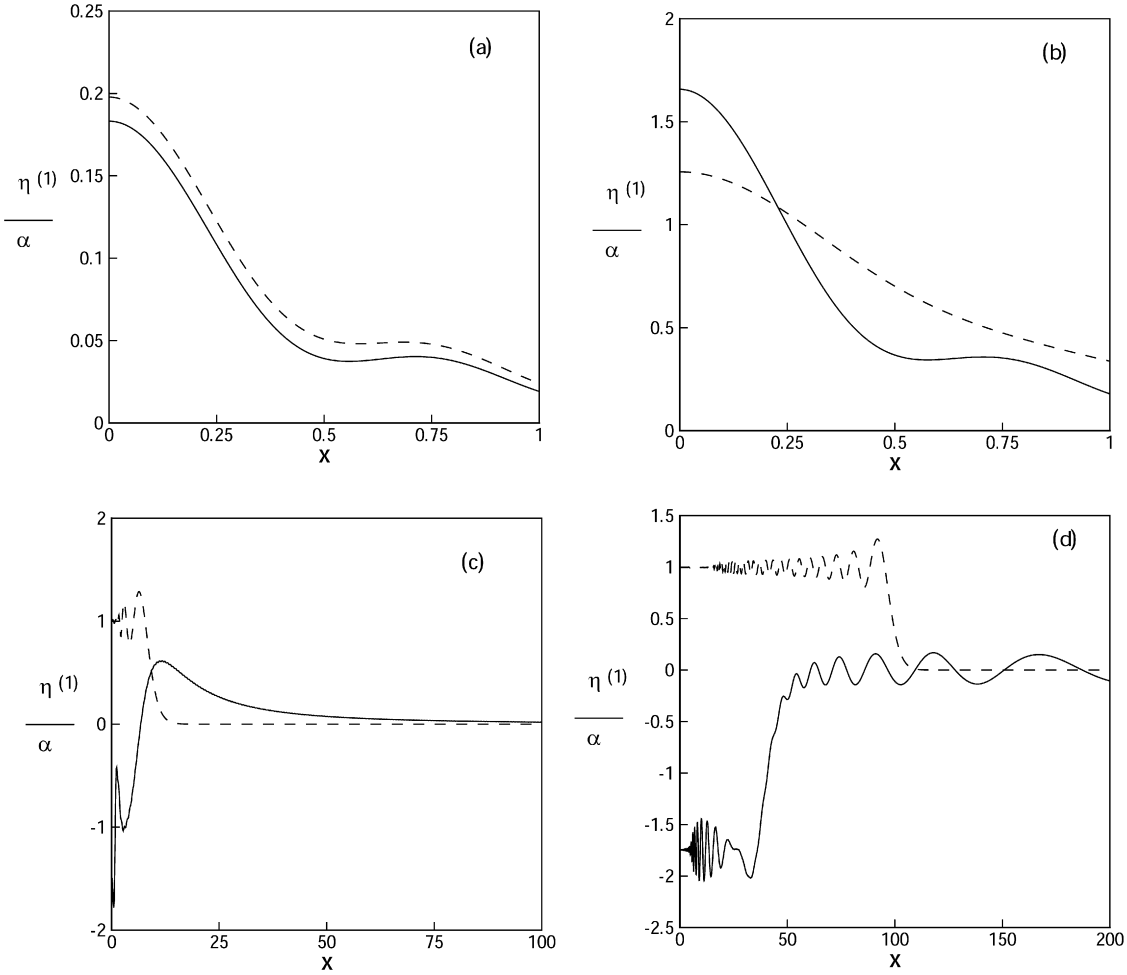

Fig. 7. Interface configuration for $u(t) = 1$ when $\rho = 0.8$, $T_1 = 2 \times 10^6$, $T_2 = 2T_1$ and $h = 1$, finite depth (- - -) and infinite depth (—). (a) $t = 0.1$; (b) $t = 1$; (c) $t = 10$; (d) $t = 100$.

wavemaker: similar curves have been given by Joo at al. [5]. However, for time becomes large, for example $t = 10$ and $t = 100$, the wave patterns are different. Unlike the case of small t, the elevation for finite depth becomes increased near the wavemaker as agreed with Joo at al. [5] while that for infinite depth becomes decreased, so the lower-layer fluid leaks under the wavemaker, and amount of oil leaking under the wavemaker becomes larger as time becomes large. This phenomenon proves that leaking under the wavemaker (or oil fence in ocean engineering) can be happened, so adjusting the position of the wavemaker submerged in the ocean becomes considerable if oil-skimming work takes longer time.

Fig. 5 shows the contact-line elevation (η at $x = 0$) with fixed density ratio and surface tension for finite depth [9] (dash line) and infinite depth (solid line) applying $h = 0.1$ and $h = 0.01$, respectively. All contact-line elevations for finite depth merely increases, which was also shown by Joo at al. [5], but different h only results to different gradient of elevation. The results of infinite depth (solid line) show different. The important point in these figures is shown when the lower-layer fluid will leak under the wavemaker with fixed h. In Figs. 5(a) and 5(b), the elevation of the surface (the interface of air and upper-layer fluid) in infinite depth results to the same with the case of finite depth, but the gradient of the elevation is lower. In Figs. 5(c) and 5(d) the elevation of the interface (the interface of upper and lower-layer fluid) initially increases, but decreases in a short time. The fact that the elevation is going under zero is important because the behavior is likely to cause oil-leaking under the wavemaker. This decreasing elevation of the interface results to the low increase of the surface elevation. As we discuss in Fig. 2, large h results to quick decrease of contact-line elevation.

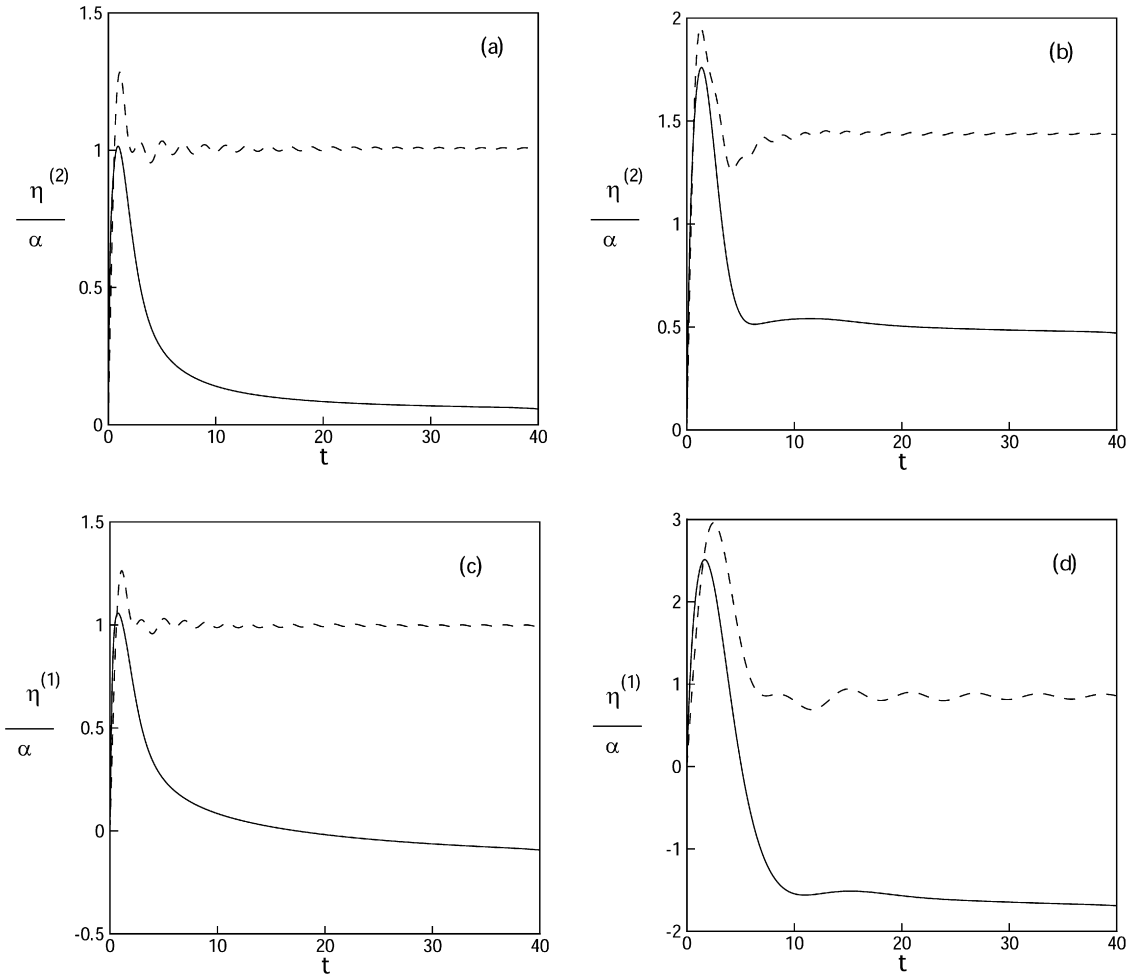

Fig. 8. Contact-line elevation for $u(t) = 1$ with $\rho = 0.8$, $T_1 = 2 \times 10^6$, $T_2 = 2T_1$: (a) and (c) $h = 0.01$ with finite depth (- - -), infinite depth (—), (b) and (d) $h = 0.1$ with finite depth (- - -), infinite depth (—).

Fig. 6 shows the interface configuration of peak time and peak location for $u(t) = t$ with various ρ and h. The value of horizontal coordinate appears inversely proportional to the value of the vertical coordinate. For large h, the wavemaker pushes more amount of fluid 1, which causes the movement of fluid 2 (oil) to be inferior, so it shortens the peak time and peak location. For large ρ, fluid 2 pushed by the wavemaker becomes pronounced, so the peak time and the peak location becomes shorter and lower, respectively. With these figures, we can estimate when the highest elevation occurs and how high the location of peak is. When we know these critical values, we can deal with oil leaking under or over the wavemaker. In Figs. 6(a) and 6(b), for example, when $h = 1$ the peak time is approximately 5 with $\rho = 0.5$ and 4 with $\rho = 0.99$, and the peak location is approximately 2.1 with $\rho = 0.5$ and 0.7 with $\rho = 0.99$. It is noted that in case of lower ρ the upper fluid movement induced by the wavemaker lasts longer, so the peak location becomes higher, which causes peck time to appear later. In Figs. 6(c) and 6(d) with fixed density ratio ($\rho = 0.5$), for example, the peak location is higher and the peak time appears later when h is smaller. We can note that smaller ρ and h causes oil leaking or oil climbing easily.

In Figs. 7–8, $u(t) = 1$; the wavemaker stays initially at rest, and is suddenly set in motion at $t = 0+$ with a constant speed Q. Fig. 7 shows interface configuration for $u(t) = 1$ with fixed surface tension and ρ for finite depth [9] (dash line) and infinite depth (solid line) from $t = 0.1$ to $t = 100$. For small t the wave pattern of infinite depth and finite depth appear similar, but the elevation of finite depth is higher; similar curves were given by Fig. 4. and Joo at al. [5]. In these figures our interesting point is when the oil leaking occurs. Unlike the case of the infinite depth, oil leaking or climbing is not observed in case of finite depth. The elevation of the interface, therefore, keeps a certain value

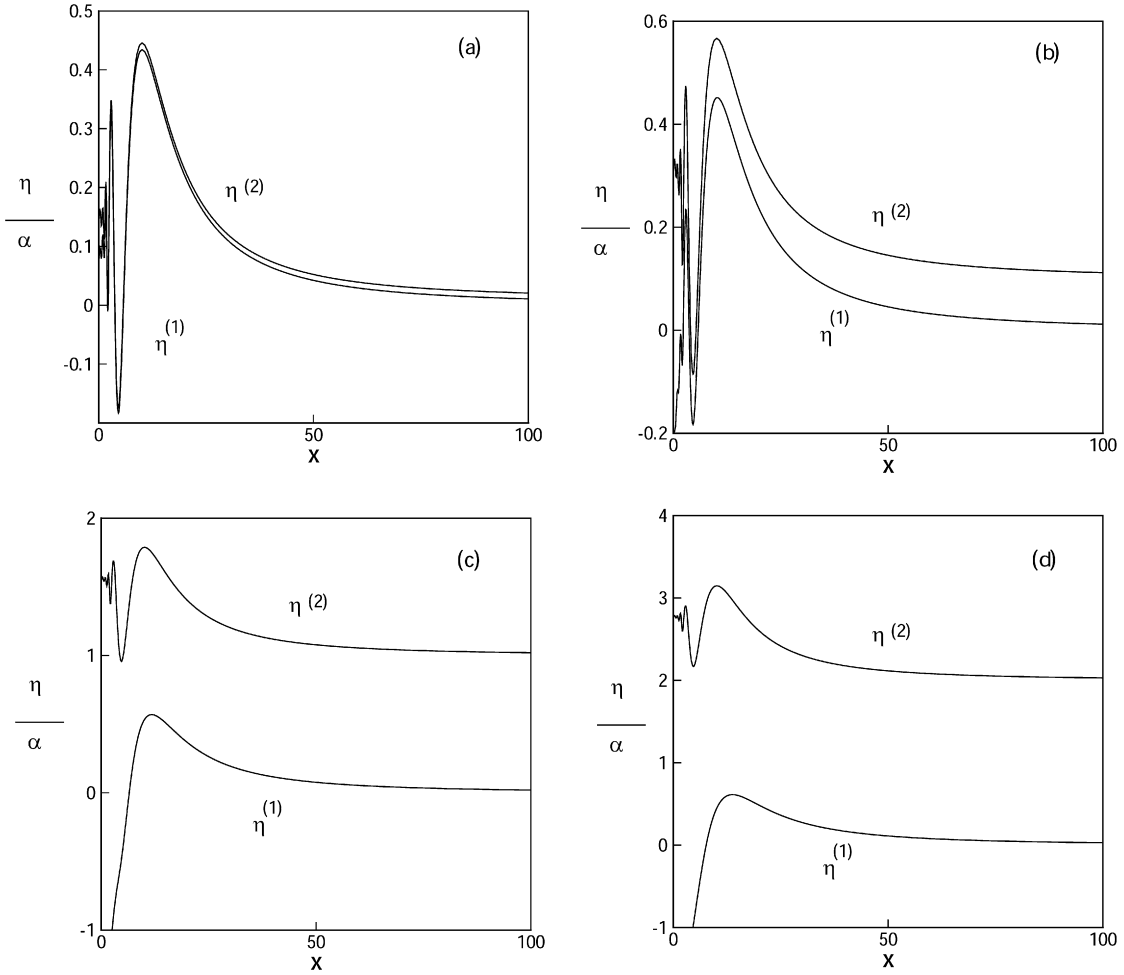

Fig. 9. Interface and free surface configuration for $u(t) = 1 - e^{-bt}$ when $t = 10$, $T_1 = 2 \times 10^6$, $T_2 = 2T_1$, $b = 1$ and $\rho = 0.8$. (a) $h = 0.01$; (b) $h = 0.1$; (c) $h = 1$; (d) $h = 2$.

near the wavemaker showing waggly motion, and far from the wavemaker, the interface appears like initial condition, which represents a typical oil-skimming behavior by the oil skirt (or wavemaker). In infinite depth, the elevation at the contact-line initially increases, however, as time becomes large, it decreases and then keeps a certain value, which represents that the possibility of oil-leaking grows.

Fig. 8 shows contact-line elevation with fixed ρ and surface tension for $h = 0.01$ and $h = 0.1$ in case of finite depth [9] (dash line) and infinite depth (solid line). For small time in both cases, the contact-line elevation urgently increases, decreases, and then becomes stable to a certain value, where the elevation in case of infinite depth is located lower than that in case of finite depth because of lower fluid leaking under the wavemaker, different from the case of the finite depth. Moreover, we can expect that contact-line elevation with large h appears initially higher and then turns to be lower under zero, which proves that the upper fluid is possible to leak under the wavemaker as h increases. These result is similar to the result of Fig. 7.

In Figs. 9–14 a more realistic wavemaker motion is considered by writing $u(t) = 1 - e^{-bt}$; the wavemaker has a finite jump in acceleration at $t = 0$, and approaches a constant value as $t \to \infty$. With t fixed, if $b \to 0$ the elevation equations approach the solution for $u(t) = t$ with α replaced by αb, and if $b \to \infty$, they approach the solution of $u(t) = 1$. The first term of the elevation equations is identical to that for $u(t) = t$, and the other term decays to zero as $t \to \infty$. Consequently, as $t \to \infty$, the behavior of fluids eventually follows that of $u(t) = 1$ regardless of the startup process. As $t \to 0$ a special case arises when $b \to \infty$ such that bt becomes constant in the limit; the solution then

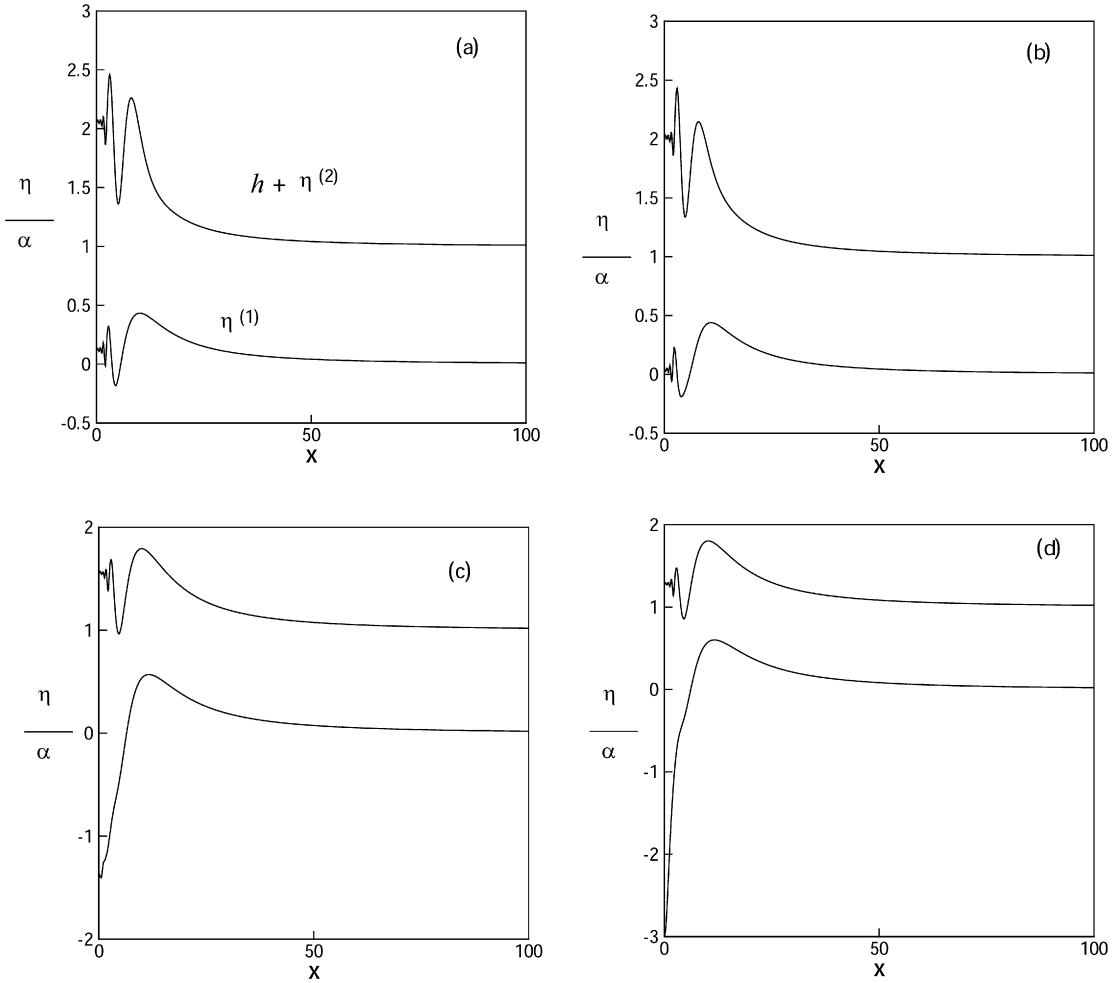

Fig. 10. Interface and free surface configuration for $u(t) = 1 - e^{-bt}$ when $t = 10$, $T_1 = 2 \times 10^6$, $T_2 = 2T_1$, $b = 1$ and $h = 1$. (a) $\rho = 0.01$; (b) $\rho = 0.1$; (c) $\rho = 0.8$; (d) $\rho = 0.99$.

depends on the value of bt. If $bt \to 0$ or $bt \to \infty$, as $t \to 0$, the small-time solution is respectively recovered for $u(t) = t$ or $u(t) = 1$.

Fig. 9 shows the interface and free surface configuration with fixed ρ, surface tension, $b = 1$ and $t = 10$ when $h = 0.01$, 0.1, 1 and 2. The fluctuation of surface elevation abruptly becomes waggly near $x = 0$ for small h. As h increases, the fluctuation of free-surface elevation becomes less waggly, and far from the wavemaker the elevation of the two interfaces becomes stable. The interesting point we can observe is that for small h ($h = 0.01, 0.1$) the amplitudes limit in the range of the wavemaker, so no leaking occurs as shown in Figs. 9(a) and 9(b), but for large h ($h = 1, 2$) the amplitudes comes over the range of the wavemaker, so the upper-layer fluid start leaking under the wavemaker. The conditions about leaking under the wavemaker will be discussed showing other figures.

Fig. 10 shows the interface and free surface configuration with fixed h, surface tension, $t = 10$ and $b = 1$ for a various ρ ($\rho = 0.01, 0.1, 0.8$ and 0.99). As shown in Fig. 3, small ρ causes the upper-layer fluid to climb the wavemaker while large ρ causes the upper-layer fluid to descend, therefore, leak under the wavemaker. The different point comparing with Fig. 3 is waggly interfaces near $x = 0$. In Fig. 10(d) the free surface elevation for unity density ratio approaches to the result of Joo at al. [5].

Fig. 11 shows the free surface configuration with a fixed ρ, surface tension, $h = 1$ and $b = 1$ for $t = 100, 1000, 2000$. Numerical values of the surface tension, for seawater and typical petroleum at 70 °F, are approximately 2×10^6 and 1×10^6, respectively. The surface becomes waggly near the wavemaker, and new thickness of upper fluid is observed. As time is large the new thickness of the upper-layer fluid expends to far from the wavemaker.

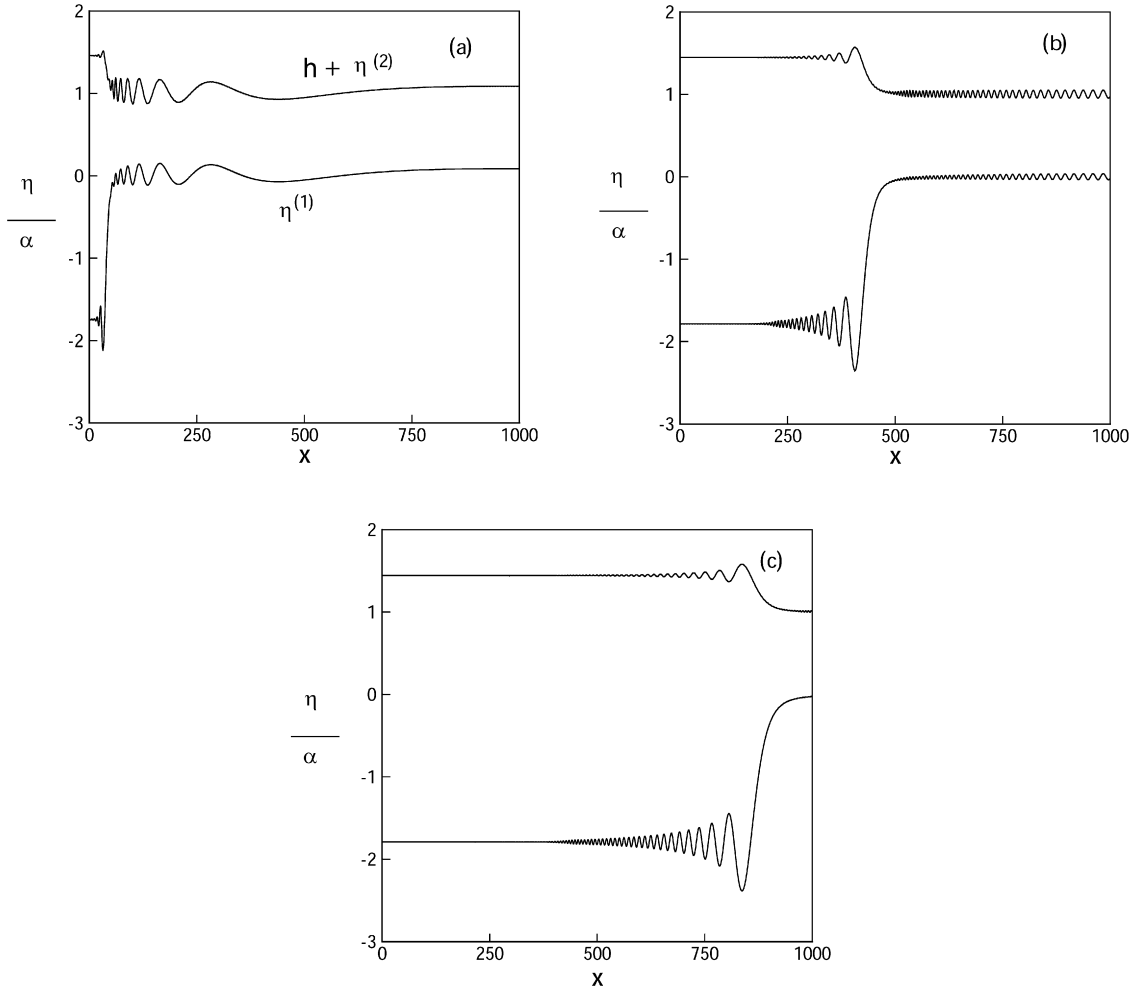

Fig. 11. Interface and free surface configuration for $u(t) = 1 - e^{-bt}$ when $\rho = 0.8$, $T_1 = 2 \times 10^6$, $T_2 = 2T_1$, $b = 1$ and $h = 1$. (a) $t = 100$; (b) $t = 1000$; (c) $t = 2000$.

This result shows similarity with oil skimming behavior in ocean engineering. Another point we should consider is the amplitude of the two contact-lines near the wavemaker. The changed contact-line elevation of the interface is more pronounced, so the upper-layer fluid is possible to leak under the wavemaker rather than climb over the wavemaker.

Because of the possibility of oil-leaking under the wavemaker, we should focus on the elevation of two interfaces as shown in Fig. 12, which shows the contact line elevation for $t \to \infty$ for three different values of ρ. The contact line elevation of free surface increases as h increases and density ratio decreases as we mentioned previously. For small ρ, the new location of the upper-layer fluid induced by the movement of the wavemaker is positioned higher than the initial location, so this condition can lead the upper-layer fluid to climb over the wavemaker. On the other hands, for large ρ, the new location of the upper-layer fluid is positioned lower, so that can lead the upper fluid layer to leak under the wavemaker. These results correspond with Sherief et al. [8]. Contact-line location shows good information to investigate if upper-layer fluid can leak under the wavemaker or climb over the wavemaker. Because the interfaces waggle near the wavemaker, considering peak location near $x = 0$ helps to observe possible oil-leaking and oil-climbing. Because of waggling interfaces, the peak location is higher than the contact line elevation in case of free surface, and the peak location is lower than the contract line elevation in case of interface. Fig. 13 shows the peak location of the interface for ($\rho = 0.8$), a representative value for water and a typical petroleum oil. Negative peak locations can provide with the possibility that the upper fluid leaks under the wavemaker. Because large h leads

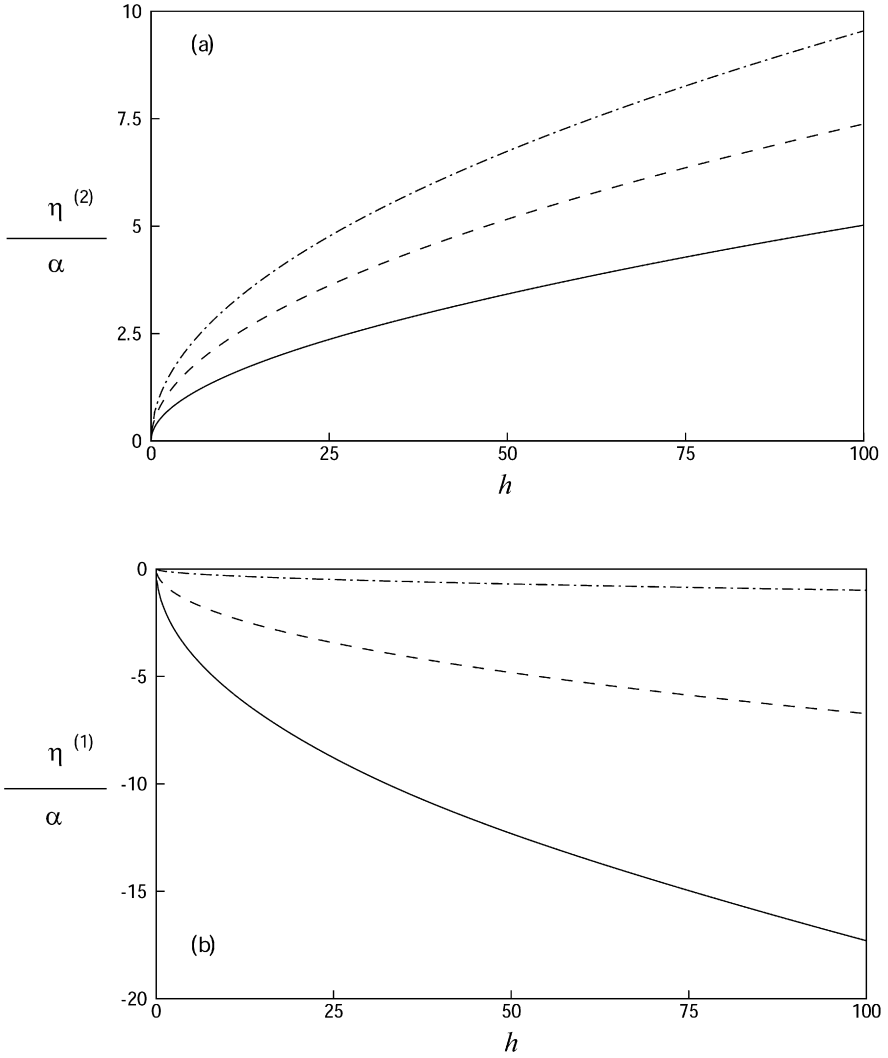

Fig. 12. Convergent contact-line elevation for $u(t) = 1 - e^{-bt}$ when $T_1 = 2 \times 10^6$, $T_2 = 2T_1$, $\rho = 0.1$ (– · –), $\rho = 0.5$ (- - -) and $\rho = 0.8$ (—).

more descendant elevation, considering the positional change of the wavemaker submerged in the two layers is more required.

Consequently, the determination of oil-leaking or oil climbing depends on the value of h and ρ. Among the two phenomena, oil leaking is more considerable in typical oil-skimming engineering. Fig. 14 shows conditions for the upper-layer of leaking under the wavemaker on a h–ρ plane. The figure supports that large ρ and lower h can cause the interface of the upper-layer fluid at the wavemaker to move downward, so the upper-layer fluid (oil) can leak under the wavemaker. In other words, if the density of the upper-layer fluid is much smaller than that of the lower-layer fluid, the area of submerged wavemaker should be more occupied at the part of upper-layer fluid because the upper-layer fluids is likely to climb over the wavemaker while if the density of the upper-layer fluid is much close to that of the lower-layer fluid, the area of wavemaker should be more occupied at the part of air (above the free surface) because the upper fluid is likely to leak under the wavemaker.

5. Concluding remarks

A method for obtaining uniformly-valid solutions is explained for a stratified fluid generated by a prescribed time-dependent motion of a vertical wavemaker which is finitely submerged, unlike Sherief et al. [8], with infinite depth

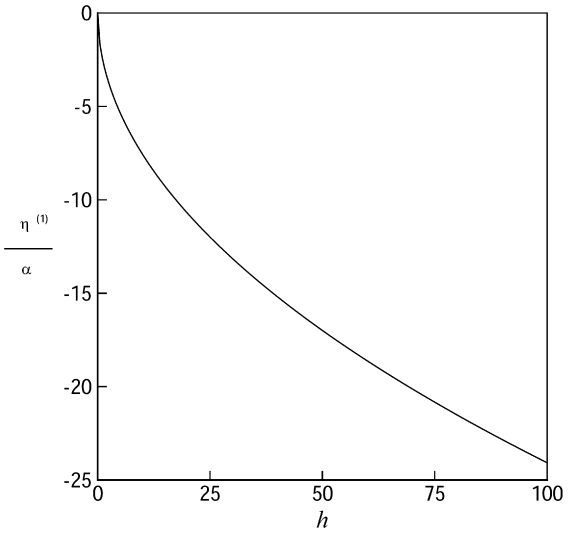

Fig. 13. Peak location of interface for $u(t) = 1 - \mathrm{e}^{-bt}$ when $\rho = 0.8$, $T_2 = 2T_1 = 2 \times 10^6$.

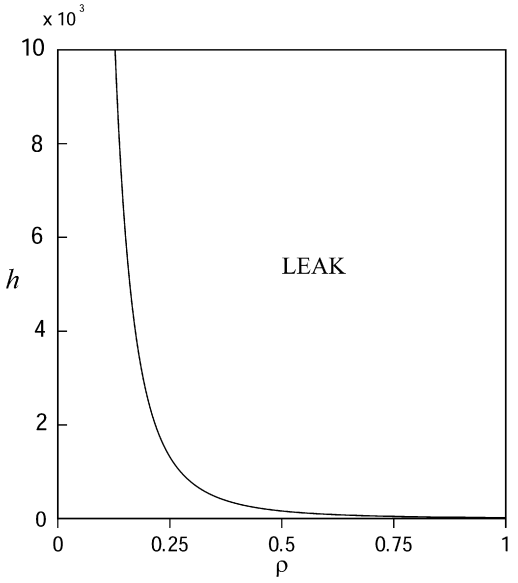

Fig. 14. Condition for "LEAK" for $u(t) = 1 - \mathrm{e}^{-bt}$ when $\alpha = 0.1$, $T_2 = 2T_1 = 2 \times 10^6$.

comparing with finite depth [9]. The artificial logarithmic singularity at the contact line appearing in the usual small-time analysis is remedied by applying the Fourier-integral approach of Joo at al. [5], which is here generalized for two fluid layers.

Various wavemaker velocities are examined in the present study. The wave motions of the interface for a small density ratio and the wave motions of the free surface for an identical density approach the results for advancing wavemaker problems in a homogeneous fluid. For any practical wavemaker motion, the method used in the present study can yield precise interfacial motions near and away from the wavemaker. The dynamics of the upper layer, including its exact spatial location for all time, thus can be accurately predicted. The conditions for the upper layer to flow past the wavemaker can be obtained, which can be useful for an oil-skimming operation.

Although the method is applicable to any general time-dependent wavemaker motions, the analysis is restricted to flows with small Froude number, which typically means small wavemaker acceleration or low wavemaker speed. If we want to perform a parametric study for the Froude number, we have to resort to other analysis than the one developed here.

Appendix A. Solutions for various wavemaker velocities $u(t)$'s

A.1. $u(t) = t$

The interface elevation is

$$\eta^{(1)} = \frac{2\alpha}{\pi} \int_0^\infty \left(\frac{n_2(\beta_1^2 c - m_1)}{s_1} \cos(\beta_1 t) - \frac{n_1(\beta_2^2 c - m_1)}{s_1} \cos(\beta_2 t) \right) \cos(kx)\, \mathrm{d}k$$

$$- \frac{2\alpha}{\pi} \int_0^\infty \frac{\rho + \mathrm{e}^{-k} - 1}{\gamma_1 k^2} \cos(kx)\, \mathrm{d}k + \mathrm{O}(\alpha^2).$$

The free surface elevation is

$$\eta^{(2)} = \frac{2\alpha}{\pi}\int_0^\infty \left(\frac{n_1(\beta_2^2 c - m_2)}{s_2}\cos(\beta_2 t) - \frac{n_2(\beta_2^2 c - m_2)}{s_2}\cos(\beta_1 t)\right)\cosh(kh)\cos(kx)\,\mathrm{d}k$$
$$- \frac{2\alpha}{\pi}\int_0^\infty \frac{1}{\gamma_2 k^2}\cos(kx)\,\mathrm{d}k + \mathrm{O}(\alpha^2),$$

where $c = \rho\tanh(kh) + 1$ and $\alpha = Q/g$.

From initial conditions we get

$$A(k,0) = 0,$$
$$A_t(k,0) = \frac{\mathrm{e}^{-k}(\rho\tanh(kh) - 1)}{2k^2(\rho\tanh(kh) + 1)} + \frac{\rho/\cosh(kh) - \rho + 1}{k^2(\rho\tanh(kh) + 1)},$$
$$A_{tt}(k,0) = 0,$$
$$A_{ttt}(k,0) = -\frac{\gamma_2\rho(\rho + \tanh(kh)/\cosh(kh) + (\tanh^2(kh) - 1)(\rho + \mathrm{e}^{-k} - 1))}{k(\rho\tanh(kh) + 1)^2}$$
$$- \frac{\gamma_1(\rho/\cosh(kh) - \rho - \mathrm{e}^{-k} + 1)}{k(\rho\tanh(kh) + 1)^2}.$$

The coefficients are

$$b_1 = A_t(k,0),$$
$$b_2 = A_{ttt}(k,0),$$
$$n_1 = \beta_1^2\left(2b_1k^2 - \mathrm{e}^{-k}\right) + 2b_2k^2,$$
$$n_2 = \beta_2^2\left(2b_1k^2 - \mathrm{e}^{-k}\right) + 2b_2k^2,$$
$$s_1 = 2\gamma_1\gamma_2k^3\left(\beta_2^2 - \beta_1^2\right)\tanh(kh),$$
$$s_2 = 2\rho\gamma_2^2k^3\left(\beta_2^2 - \beta_1^2\right)\tanh(kh),$$
$$m_1 = \gamma_2k\left(\rho + \tanh(kh)\right) + \gamma_1k,$$
$$m_2 = \rho\gamma_2k\left(\tanh^2(kh) - 1\right) - \gamma_1k.$$

A.2. $u(t) = 1$

The interface elevation is

$$\eta^{(1)} = \frac{2\alpha}{\pi}\int_0^\infty \left(\frac{n_1\beta_2(\beta_2^2 c - m_1)}{s_1}\sin(\beta_2 t) - \frac{n_2\beta_1(\beta_1^2 c - m_1)}{s_1}\sin(\beta_1 t)\right)\cos(kx)\,\mathrm{d}k.$$

The free surface elevation is

$$\eta^{(2)} = \frac{2\alpha}{\pi}\int_0^\infty \left(\frac{n_2\beta_1(\beta_1^2 c - m_2)}{s_2}\sin(\beta_1 t) - \frac{n_1\beta_2(\beta_2^2 c - m_2)}{s_2}\sin(\beta_2 t)\right)\cosh(kh)\cos(kx)\,\mathrm{d}k,$$

where $\alpha = Q/\sqrt{gd_1}$.

From initial conditions we get

$$A(k,0) = \frac{2 - \mathrm{e}^{-k}}{2k^2},$$
$$A_t(k,0) = 0,$$

$$A_{tt}(k,0) = \frac{(1-\mathrm{e}^{-k})(\gamma_2\rho\tanh^2(kh) - \gamma_2\rho - \gamma_1)}{k(\rho\tanh(kh)+1)} - \frac{\gamma_2\rho\tanh(kh)}{k\cosh(kh)(\rho\tanh(kh)+1)},$$

$$A_{ttt}(k,0) = 0.$$

The coefficients are

$$b_1 = A(k,0),$$

$$b_2 = A_{tt}(k,0),$$

$$n_1 = \beta_1^2\left(2b_1k^2 - \mathrm{e}^{-k}\right) + 2b_2k^2,$$

$$n_2 = \beta_2^2\left(2b_1k^2 - \mathrm{e}^{-k}\right) + 2b_2k^2,$$

$$s_1 = 2\gamma_1\gamma_2k^3\left(\beta_2^2 - \beta_1^2\right)\tanh(kh),$$

$$s_2 = 2\rho\gamma_2^2k^3\left(\beta_2^2 - \beta_1^2\right)\tanh(kh),$$

$$m_1 = \gamma_2k\left(\rho + \tanh(kh)\right) + \gamma_1k,$$

$$m_2 = \rho\gamma_2k\left(\tanh^2(kh) - 1\right) - \gamma_1k.$$

A.3. $u(t) = 1 - \mathrm{e}^{-bt}$

The particular solution is

$$\begin{aligned} A_p(k,t) = {} & \frac{b^4}{(a_1b^4 + a_2b^2 + a_3)k^2}\left(\frac{\mathrm{e}^{-k}}{2}\left(1 - \rho\tanh(kh)\right) - \frac{\rho}{\cos(kh)} + \rho - 1\right) \\ & + \frac{\gamma_2b^2}{(a_1b^4 + a_2b^2 + a_3)k}\left((\rho-1)\tanh(kh) + \frac{\mathrm{e}^{-k}}{2}\left(\tanh(kh) - \rho\right)\right) \\ & - \frac{\gamma_1\mathrm{e}^{-k}}{2k(a_1b^4 + a_2b^2 + a_3)}\left(\gamma_2k\tanh(kh) + b^2\right) + \frac{\mathrm{e}^{-k}}{2k^2}. \end{aligned}$$

The interface elevation obtained is

$$\begin{aligned} \eta^{(1)} = {} & \frac{2\alpha}{\pi}\int_0^\infty\left(\frac{\beta_1(\beta_1^2c - J_1)}{2\gamma_1\gamma_2k^2J_2}J_0\sin(\beta_1t) - \frac{\beta_1^2c - J_1}{\gamma_1\gamma_2J_2}J_3\cos(\beta_1t)\right)\cos(kx)\,\mathrm{d}k \\ & - \frac{2\alpha}{\pi}\int_0^\infty\left(\frac{\beta_2(\beta_2^2c - J_1)}{2\gamma_1\gamma_2k^2J_2}J_4\sin(\beta_2t) - \frac{\beta_2^2c - J_1}{\gamma_1\gamma_2J_2}J_5\cos(\beta_2t)\right)\cos(kx)\,\mathrm{d}k + \frac{2\alpha}{\pi}\int_0^\infty B_p(k,t)\cos(kx)\,\mathrm{d}k. \end{aligned}$$

The free surface elevation is

$$\begin{aligned} \eta^{(2)} = {} & -\frac{2\alpha}{\pi}\int_0^\infty\left(\frac{\beta_1(\beta_1^2c - J_6)}{2\gamma_2^2k^2\rho J_2}J_0\sin(\beta_1t) - \frac{\beta_1^2c - J_6}{\gamma_2^2\rho J_2}J_5\cos(\beta_2t)\right)\cosh(kh)\cos(kx)\,\mathrm{d}k \\ & + \frac{2\alpha}{\pi}\int_0^\infty\left(\frac{\beta_2(\beta_2^2c - J_6)}{2\gamma_2^2k^2\rho J_2}J_4\sin(\beta_2t) - \frac{\beta_2^2c - J_6}{\gamma_2^2\rho J_2}J_5\cos(\beta_2t)\right)\cosh(kh)\cos(kx)\,\mathrm{d}k \\ & + \frac{2\alpha}{\pi}\int_0^\infty D_p(k,t)\cos(kx)\,\mathrm{d}k, \end{aligned}$$

where $\alpha = U_0/(gh)^{1/2}$.

From initial conditions we get

$$A(k,0)=0,$$

$$A_t(k,0)=\frac{b\mathrm{e}^{-k}(\rho\tanh(kh)-1)}{2k^2(\rho\tanh(kh)+1)}+\frac{b(\rho/\cosh(kh)-\rho+1)}{k^2(\rho\tanh(kh)+1)},$$

$$A_{tt}(k,0)=-\frac{b^2(\mathrm{e}^{-k}(\rho\tanh(kh)-1)+2\rho/\cosh(kh)+2-2\rho)}{2k^2(\rho\tanh(kh)+1)},$$

$$\begin{aligned}A_{ttt}(k,0)=&\frac{b^3}{2k^2(\rho\tanh(kh)+1)^2}\left(\mathrm{e}^{-k}\left(\rho^2\tanh^2(kh)-1\right)-2-2\rho\right)\\&+\frac{b^3\rho}{k^2(\rho\tanh(kh)+1)^2}\left(\frac{\rho\tanh(kh)+1}{\cosh(kh)}+(1-\rho)\tanh(kh)\right)\\&+\frac{\gamma_2 b\rho}{k^2(\rho\tanh(kh)+1)^2}\left((\tanh^2(kh)-1)J_7-\frac{\rho+\tanh(kh)}{\cosh(kh)}\right)\\&-\frac{\gamma_1 b}{k(\rho\tanh(kh)+1)^2}\left(\frac{\rho}{\cosh kh}+J_7\right).\end{aligned}$$

The coefficients are

$$B_p(k,t)=\frac{b\tanh(kh)}{a_4}J_7\mathrm{e}^{-bk}+\frac{b^3}{ka_4}\left(J_7+\frac{\rho}{\cosh(kh)}\right)\mathrm{e}^{bt},$$

$$D_p(k,t)=\frac{b^3}{ka_4}\left[J_7\left(1-\tanh^2(kh)\right)+\frac{\rho+\tanh(kh)}{\cosh(kh)}t\right]\cosh(kh)\mathrm{e}^{-bt}+\frac{b\gamma_1}{a_4}\tanh(kh)\mathrm{e}^{-bt},$$

$$a_4=b^4a_1+b^2a_2+a_3,$$

$$J_0=\beta_2^2\left(2A_pk^2+\mathrm{e}^{-k}\right)+2A_pb^2k^2-2P_2k^2,$$

$$J_1=\gamma_2k\left(\rho+\tanh(kh)\right)+\gamma_1k,$$

$$J_2=\left(\beta_1^2-\beta_1^2\right)k\tanh(kh),$$

$$J_3=\beta_2^2(A_p+P_1)+A_pb^3+P_3,$$

$$J_4=\beta_1^2\left(2A_pk^2+\mathrm{e}^{-k}\right)+2A_pb^2k^2-2P_2k^2,$$

$$J_5=\beta_1^2(A_pb+P_1)+A_pb^3+P_3,$$

$$J_6=\gamma_2k\rho\tanh^2(kh)-\gamma_2k\rho-\gamma_1k,$$

$$J_7=1-\rho-\mathrm{e}^{-k},$$

$$A_p=A_p(k,t)\mathrm{e}^{bt},$$

$$P_1=A_t,$$

$$P_2=A_{tt},$$

$$P_3=A_{ttt}.$$

References

[1] D.H. Peregrine, Flow due to a vertical plate moving in a channel, Unpublished note, 1972.
[2] A.T. Chwang, Nonlinear hydrodynamic pressure on an accelerating plate, Phys. Fluids 25 (1983) 383–387.
[3] W.M. Lin, Nonlinear motion of the free surface near a moving body, Ph.D. Thesis, MIT, Dept. of Ocean Engineering, 1984.
[4] A.J. Roberts, Transient free-surface flows generated by a moving vertical plate, Quart. J. Mech. Appl. Math. 40 (1987) 129–158.
[5] S.W. Joo, W.W. Schultz, A.F. Messiter, An analysis of the initial-value wavemaker problem, J. Fluid Mech. 214 (1990) 161–183.

[6] A.C. King, D.J. Needham, The initial development of a jet caused by fluid, body and free-surface interaction. Part 1. A uniformly accelerating plate, J. Fluid Mech. 268 (1994) 89–101.
[7] P.F. Rhodes-Robinson, On wave motion in a two-layered liquid of infinite depth in the presence of surface and interfacial tension, J. Aust. Mech. Soc. Ser. B 40 (1994) 129–158.
[8] H.H. Sherief, M.S. Faltas, E.I. Saad, Forced gravity waves in two-layered fluids with upper fluid having a free surface, Canad. J. Phys. 81 (2003) 675–689.
[9] S.W. Joo, M.S. Park, Wave motions in stratified fluids by a translating plate, J. Mech. Sci. Technol. 20 (6) (2006) 883–896.
[10] T.H. Havelock, Forced surface-wave on water, Philos. Mag. 8 (1980) 569–579.
[11] W.H. Press, S.A. Tenkolsky, W.T. Vetterling, B.P. Flannery, Numerical Recipes, second ed., Cambridge Univ. Press, 1992.